Effective Time Constants at 4.2 to 70 K in *Re*BCO Pancake Coils With Different Inter-Turn Resistances

T. H. Nes, G. De Rijk, G. Kirby, F. O. Pincot, J. Liberadzka-Porret, C. Petrone, S. C. Richter, J. van Nugteren, A. Kario, and H. H. J. Ten Kate, *Senior Member, IEEE*

***Abstract*—For future *Re*BCO tape based accelerator magnets it is proposed to use no- or partial inter-turn insulation to deal with quench detection and protection. In a non-insulated coil the turns are separated by a finite electrical resistance, providing a bypass for the current at hot-spots, improving thermal stability and quench detection time. However, such coils show different dynamic electromagnetic behavior compared to insulated coils under normal charging and transient quench conditions. To study such coils in detail two pancake coils, one dry-wound and one with solder in between turns, are prepared and tested in a variable temperature cryostat between 4.2 and 70 K. Properties of the coils that are studied are charge and discharge time behavior, turn-to-turn resistance, response to current stepping, and operational stability. In this paper, the first results are presented and compared to a simplified network model in order to gain further understanding into the underlying physics.**

***Index Terms*—High-temperature superconductors, network model, *Re*BCO, superconducting coils, time constant.**

I. Introduction

FOR magnets made from high-temperature superconductor (HTS) rare-earth barium copper oxide (*Re*BCO) conductors, one of the main problems is the protection of the magnet in the case of a quench. Two strategies can be discerned to manage this: actively by instrumenting the coil so that the onset of a quench is detected and proper action is taken, and passively by changing the coil's inter-turn resistance to accommodate the occurrence of a quench safely. Here, a passive strategy is investigated, by which the coil winding pack of the magnet is made non-insulated by separating the turns with a finite resistance [1]. In a local normal zone, the current can bypass the defective spot through the finite resistance to the next turns (see Fig. 1) [2].

Manuscript received September 27, 2021; revised December 14, 2021; accepted January 24, 2022. Date of publication February 7, 2022; date of current version March 1, 2022. *(Corresponding author: Thomas Nes.)*

T. H. Nes is with the University of Twente, 7522 NB Enschede, Netherlands, and also with the CERN, 1211 Geneva, Switzerland.

G. De Rijk, G. Kirby, F. O. Pincot, J. Liberadzka-Porret, C. Petrone, and S. C. Richter are with the CERN, 1211 Geneva, Switzerland.

J. van Nugteren was with the CERN, Meyrin, Geneva 1211, Switzerland, and is now with the Little Beast Engineering Sàrl, 1272 Genolier, Switzerland.

A. Kario and H. H. J. Ten Kate are with the University of Twente, 7522 NB Enschede, Netherlands.

Color versions of one or more figures in this article are available at https://doi.org/10.1109/TASC.2022.3148968.

Digital Object Identifier 10.1109/TASC.2022.3148968

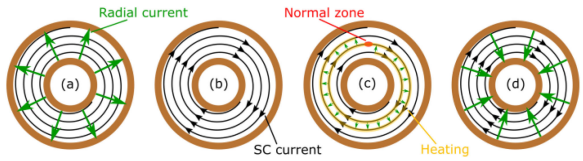

Fig. 1. Predicted current path in the case of (a) charging the coil, (b) operation in steady state, (c) in the presence of a normal zone, and (d) during discharge.

The drawback of non-insulated coils is the much higher time constant compared to their insulated counterparts, due to the existence of a non-superconducting current path, leading to longer charging and discharging times. Consequently, in the design of the coil, a trade-off has to be made between stability and the effective time constant of the coil, depending on the requirements set by the coil's application.

Various research groups have employed various non-insulation strategies. "Dry-wound", where there is no insulation material between the turns and the copper coatings of adjacent *Re*BCO tapes are directly in contact [3]. "Soldered", where solder is added between the turns [4]–[6]. "Metal-insulated", where a metal strip is co-wound between the tapes [7]–[10]. Another variant is applying metal cladding, where a metallic coating is added to the *Re*BCO tape [11]–[14]. Also conductive epoxy has been tried as an interstitial material [15]. This work aims to perform a comparative study between similar sized coils with different inter-turn configurations.

This paper presents the construction and test results of two dimensionally identical small pancake coils made with two different coil winding pack configurations: dry-wound and soldered. The dry-wound was wound first, to have a first experience with winding *Re*BCO tape. Then the soldered coil was wound by adding solder between the turns during winding. The soldered coil is expected to have a lower inter-turn resistance [4]. The results are compared with a theoretical prediction based on a network model. The coils are tested at different temperatures between 10 and 70 K in a variable flow cryostat, where the flow of helium gas is controlled to reach the desired temperature, and the dry-wound coil is tested in liquid helium at 4.2 K. The lessons learnt from the small coil program is used in other *Re*BCO-HTS projects at CERN such as the first of its kind cloverleaf type dipole accelerator magnet [16], [17], a new magnetic spectrometer demonstrator magnet for use in space (HDMS) [18], a novel toroidal magnet for a gantry for hadron therapy [19], and undulator coils for compact free-electron lasers [20].

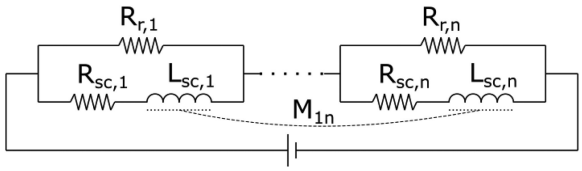

Fig. 2. Schematic of the network model. The current in a turn can flow radially between turns via the radial resistance R_r, or azimuthally through the superconductor, which has resistance R_{sc} corresponding to the superconducting-to-normal transition, self-inductance L_{sc} and mutual inductance M_{sc}.

II. Network Model

Various network models have been used by authors to simulate the performance of non-insulated coils. The most basic one is a lumped model, first proposed by Hahn *et al.* [1], [3] where two parallel paths describe the whole coil, one azimuthal path corresponding to the superconductor with a self-inductance and azimuthal resistance, and a radial path with a radial resistance. This was expanded by Bhattarai *et al.* [21] to model a multi coil configuration. To model local current distributions, distributed models are used, where the windings are divided in multiple sub-sections [22]–[25].

Here, an intermediate distributed model is proposed, which can be solved analytically. The aim of the network model is to predict the temporal behaviour of the voltage over the whole coil and coil segments as function of time for different powering cases. The equivalent network is shown in Fig. 2. In this model, each turn is a node with an azimuthal and a radial path. The system has *n* nodes, which corresponds to *n* turns in the coil. One path corresponds to the current flowing through the superconductor. It consists of a self-inductance and mutual inductances with the other turns, and a variable resistance corresponding to the superconducting-to-normal state transition. The other path corresponds to the radial path, and consists of a resistance. Using Kirchhoff's circuit laws, the system of equations to be solved for the entire system is:

$$\frac{dI_{sc}}{dt} = M^{-1}\left(I_p R_r - I_{sc}\left(R_r + R_{sc}\right)\right), \tag{1}$$

where $\boldsymbol{I}_{sc}$ is the current carried by the superconductor in each turn, $\boldsymbol{M}$ is the inductance, $\boldsymbol{I}_p$ is the current introduced by the power supply, $\boldsymbol{R}_r$ is the radial resistance and $\boldsymbol{R}_{sc}$ is the variable resistance of the superconductor. The bold font indicates that we are dealing with a matrix, non-bold italics are reserved for scalars. The inductance matrix can be calculated using computer codes or look-up tables [26]. The resistance matrix can estimated using first order approaches based on the geometry of the coil, and refined using the measurement data. The refinement is required, as the radial resistance is influenced by interstitial material [1], winding tension [27] and the transversal resistance of the *Re*BCO tape [14]. $\boldsymbol{R}_{\mathrm{sc}}$ is intended to be parameterised with a fit function, but for these experiments it is provisionally put to be equal to zero, the pure superconducting case, to be able to solve Eq. (1) analytically. In terms of voltage, Eq. (1) can be rewritten as:

$$\frac{dU}{dt} = -{\Theta_c}^{-1} U, \tag{2}$$

where we define $\Theta_c = \boldsymbol{M}\boldsymbol{R}^{-1}$ as the time constant matrix. This matrix definition is analogous to the lumped approach, where the time constant is defined in terms of scalars as $\tau = L/R$ [3].

TABLE I
Coil Parameters

Parameter	Dry-wound	Soldered
Turns	268	261
Inner diameter	52 mm	52 mm
Outer diameter	102.1 ± 0.1 mm	102.3±0.3 mm
Calculated inductance	5.9 mH	5.6 mH
Radial resistance (300 K)	1.0 mΩ	570 μΩ

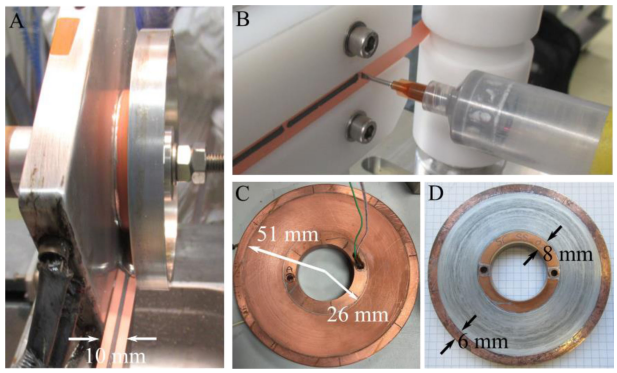

Fig. 3. Pictures of (A) winding the soldered-coil, (B) applying solder paste to the tape, (C) dry-wound and (D) soldered coil.

The general solution to Eq. (2) can be written as:

$$U = U_0 \ e^{-{\Theta_c}^{-1} t} = \sum_{k=1}^{n} c_k e^{-\lambda_k t} \Lambda_k, \tag{3}$$

where λ and Λ are the eigenvalues and eigenvectors of the inverse of the time constant matrix Θ_c, and $c = \Lambda^{-1} U_0$ constants depending on the initial conditions of the system. For an applied current step when the voltage over the coil is zero, the voltage response can be described as

$$U = I_{p0} R_r e^{-{\Theta_c}^{-1}(t-t_0)}, \tag{4}$$

where $\boldsymbol{I}_{p0}$ is the size of the current step applied at t_0 by the power supply, and can be both positive and negative.

III. Coil Manufacturing and Test Set-up

A. Coil Winding and Assembly

Two pancake coils were wound and assembled, a dry-wound and a soldered coil. In Table I, their key parameters are listed. For both coils 10 mm wide, 95 μm thick *Re*BCO tape from Shanghai Superconductor Technologies is used featuring a substrate thickness of 50 μm, a copper layer thickness of 20 μm per side, and a critical current at 77 K, self-field of 400 A [29]. In Fig. 3, the coil winding and instrumentation is shown.

The construction of both coils starts with the inner copper ring on which the superconductor tape is wound. The tape is fixed in a slot in the inner copper ring, which assures that it cannot be pulled out. A low winding tension of 33 N was chosen for the winding tension to avoid damaging the tape. The coil turns are then wound around the inner copper ring, until an outer diameter of 102 mm is reached. The outer copper ring is subsequently heat shrunk fit around the coil winding pack.

For the dry-wound coil, the first and last turns are soldered using Sirius 1D Sn62Pb36Ag2 solder to the copper. The solder

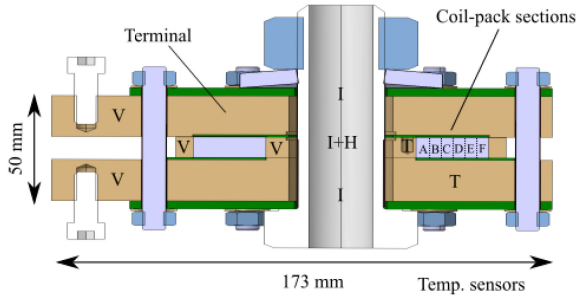

Fig. 4. Schematic of the coil's enclosure. The coil is divided into six equally spaced sections. A voltage trace is used to measure the voltage over each individual section. Instrumentation: T = temperature sensor, V = voltage tap, I = induction coil and H = Hall probe.

is required to be in the form of a paste with a melting temperature below 200 °C to avoid tape degradation by overheating. For the soldered coil, Sirius 1D solder is added between the turns using a syringe, and the solder is pushed out at a continuous rate by pressurizing the top of the syringe with an overpressure of 1.5 bar. The coil is clamped between a heating plate and a metal flange. The heating plate is heated up to 180 °C for the solder to melt. The coil is wound warm taking about an hour.

Good contact with a homogeneous pressure between the copper rings and the terminals is obtained using polyimide shimming. Fuji paper is used in the pre-assembly to determine the magnitude and distribution of the pressure between the rings and the terminal plates, such that electrical contact is ensured in the final assembly. The coil is then assembled in its enclosure. A schematic sketch is given in Fig. 4. The coil is clamped between two copper terminals, to which the current leads are attached. The terminals act as current inputs and as a thermal stabilizer. Indium foil is placed between the copper rings and the terminals for a good electrical contact.

B. Instrumentation and Measurement Set-Up

The coil is instrumented with a voltage tap on each copper ring and a carbon ceramic temperature sensor (CCS) in the inner copper ring [28]. A second CCS sensor is placed inside one of the terminals, and a voltage pair is placed on the terminals for measuring the entire coil voltage. A voltage trace is placed on one edge surface of the coil winding pack for the soldered coil. The trace consists of 16 voltage taps, of which 14 are radially distributed on the coil winding pack and two on the outer copper ring. The radial voltage taps divide the coil in six sections (labelled here A to F), where each section corresponds to $1/6^{\text{th}}$ of the coil winding pack, and where section A is on the inside of the coil winding pack (see Fig. 4). The trace also comprises a compensation coil to measure the voltage over the full coil with cancellation of the inductive component. The radial voltage taps are used to read the voltage on the coil at different positions. The magnetic measurement is performed by using the induction coil and a Hall probe positioned in the bore of the magnet, whereby the central induction coil is used to calibrate the Hall probe.

The coils are tested in a variable flow cryostat. In the bottom of the cryostat, an evaporator boils off liquid helium. This flow passes a flow conditioner, which heats up the gas controlled to the desired temperature of the coil.

IV. Results and Discussion

A. Effective Time Constant

The effective time constant is an indicator of the time it takes for the current to enter and exit the superconductor [1]. From Eq. 3, it can be seen that the voltage decay following a current step over the full coil is a summation of exponents with different decay constants λ_k. Instead of summing all the terms in Eq. 3, the voltage decay can be approximated considering only the first two terms:

$$U \approx a_1 e^{-t/\tau_i} + a_2 e^{-t/\tau_a vg}, \tag{5}$$

where a_1 and a_2 are constants depending on the initial condition and τ_i and τ_{avg} are the effective time constants, corresponding to the initial and average decay response of the system. In comparison with Eq. 3, these time constants are the two largest eigenvalues of the time constant matrix. The time it takes to enter the superconductor τ_{avg} corresponds to the largest eigenvalue of the time constant matrix. The average effective time constant will be considered in the rest of the paper, as this determines the ramping time of the magnet.

Here this value is determined using a current step-down. By fitting Eq. 5 to the measured coil decay, τ_{avg} is determined. In Fig. 5, τ_{avg} for both coils is plotted as a function of temperature. It can be seen that at 30 K the time constant of the dry-wound coil drops considerably. The measurements were repeated at 68 K, and the time constant was found a factor 10 lower compared to the first measurements at this temperature, indicating an irreversible increase in the inter-turn-resistance. The measured critical current was the same for both measurements at 68 K. At present the reason for this is not well understood. Hypothetical explanations are a changing contact resistance due to Lorentz forces or damage to the copper coating due to the radial currents. For the soldered coil, this behaviour in the effective time constant is not observed. Between 77 K and 10 K, τ_{avg} of the soldered coil becomes a factor of four larger. Between the dry-wound coil and the soldered coil, there is a factor of 40 difference at 70 K at the start of the measurement campaign, and a factor of 400 at the end of the measurement campaign. At 10 K the average time constant differs by a factor of 1600.

B. Current Step and Overshoot

In Fig. 6, the voltage response of sections A to C of the soldered coil is shown when a current step down of 300 A is applied at 50 K. Based on critical current measurements of the SST tape performed by the University of Wellington [30], at this temperature, the critical current was expected to be 450 A. Right after the current step, the current flow can be approximated with the scheme in Fig. 1(a), where most current flows radially. When the voltages have decayed completely, all current has settled in the superconductor (Fig. 1(b)). When the current is stepped down, the current flows as shown in Fig. 1(d). The negative voltage during the step-down is due to the radial current flowing in the opposite direction compared to charging.

The charging time can be reduced by applying an overshoot method [31]. In Fig. 7, an overshoot of 760 A is applied to the soldered coil at 50 K, thereby reducing the charging time by a factor of five. The radial current behaviour is more dynamic than in the case of a single step. When the current is stepped down with 300 A, it can be seen that some sections have a positive voltage, and other sections show negative voltages. This means

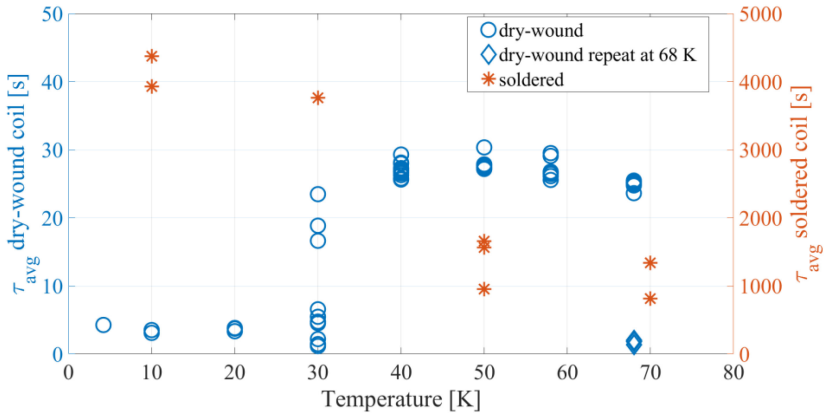

Fig. 5. Evolution of the effective time constant τ_{avg} of both coils plotted as function temperature. The individual data-points correspond to individual measurements. For the dry-wound coil, the effective time constant drops suddenly around 30 K. When the experiments were repeated at 68 K, the effective time constant did not recover. For the soldered coil, the effective time constant increases with decreasing temperature.

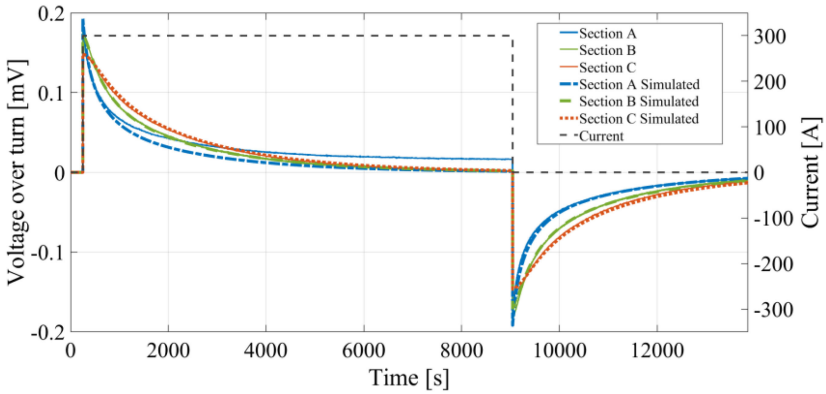

Fig. 6. Voltage across coil sections of the soldered coil to a current step-up and step-down of 300 A as a function of time, for the sections on the inside of the coil, at 50 K. The measurement data are compared to simulation data, and shows good agreement for sections B and C, but not for A.

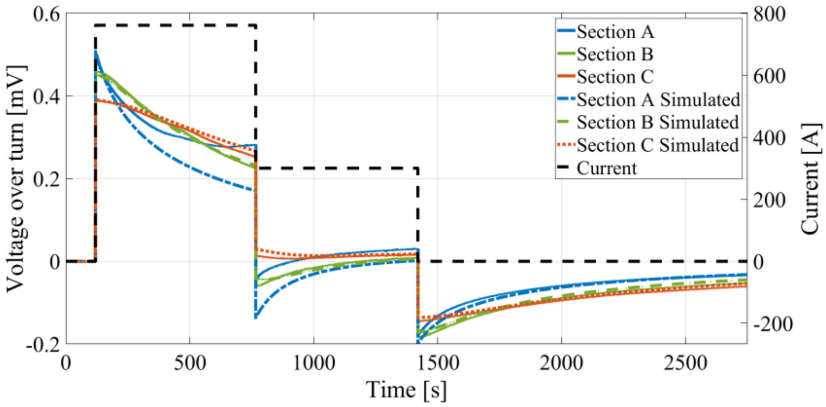

Fig. 7. Voltage across coil sections versus time showing the overshoot response of the soldered coil to a current step at 50 K. First a current of 762 A is applied. At t = 766 s, the current is stepped down to 300 A. The measured data is compared to simulated data, and shows good agreement for sections B and C. For section A, the model significantly deviates.

that in some sections the radial current is flowing in the opposite direction from other sections.

The measurements are compared to a simulation with the presented network model. The inductance matrix is calculated using FIELDS [32], given the geometry of the coil as input. Each spiral turn of the coil is simulated as a circle of 10 mm width and 2 μm thickness, approximating the geometrical shape of the superconductor. A best-fit value of the model for the coil average resistivity ρ_{coil}, giving the best overlap with the measured data in the powering cases shown in Figs. 6 and 7, is 58 μΩ•m. The basic formula for the resistance is $R = \rho L/A$, where ρ is the resistivity, A is the surface area and L the length along which

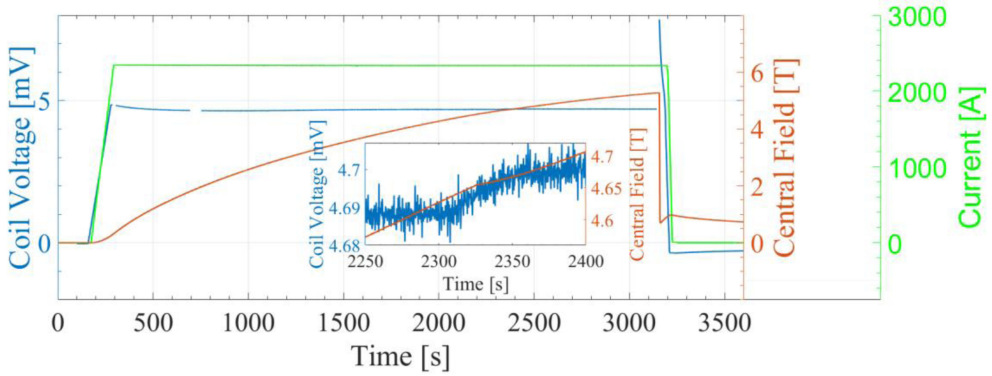

Fig. 8. Magnetic field and current versus time. Response of the soldered coil to a current step of 2.4 kA at 10 K. A quench can be observed at t ≈ 3200 s. After the quench, the coil starts to repower until the current was cut manually.

the current is flowing. For an annular configuration as the small solenoid, where the resistive current flows radially through the annulus, this formula then becomes by integration:

$$R_{r,ii} = \rho_{coil} * \ln\left(r_{i+1}/r_i\right)/2\pi w, \tag{6}$$

where $R_{r,ii}$ are the diagonal elements of the resistance matrix, r_i is the radius of the i^{th} turn, and w is the width of the tape. For sections B and C, the network model shows good agreement with the measured data. For section A however, the model is not in agreement with the simulation. As this section is closest to the copper rings, heating of the inner copper ring may generate a voltage over the first turns. To model accurately, more advanced network models are required, which include effects such as joule heating, thermal propagation and superconducting to normal state transitions.

C. Self-Protection

Fig. 8 shows the voltage and magnetic field responses to a current step of 2.4 kA of the magnetic flux density as a function of time. The measurement was performed on the soldered coil at 10 K. At this temperature, the expected critical current is 1.7 kA. When the coil is fully charged, the coil is thus expected to run in overcurrent. At t ≈ 3200 s, a quench can be observed, with a corresponding sharp drop in magnetic field. A possible explanation can be the following. Due to the lower self-inductance of the inner turns they charge first. This can also be observed in Fig. 7, where the inner section voltage drops faster than those of the outer sections. As the outer turns fill up later, the magnetic field on the inner turns is increased, lowering the critical surface of the tape in these sections. If the turns were carrying more current than the critical current, this current now needs to be expelled radially, leading to a local increase in temperature, thereby lowering the critical current density even further. If the heat load is too big, this cascades into a quench. At t ≈ 2300 s, one can observe that the ramp up is not smooth, as can be seen in the insert in Fig. 8. The coil does not quench completely, as the magnetic field does not drop to zero. When the coil has cooled down sufficiently, the coil starts to recharge. This is an example of self-protection. The power supply was shut off a bit later. Quenches were observed below 30 K for the dry-wound coil, but these were not self-recoverable, as the temperature did rise too high during the quench.

V. Conclusion

A versatile system to measure the temporal behavior of voltages over non-insulated *Re*BCO pancake coils and magnetic field was developed, where coils with a similar geometry but with a different inter-turn-resistance can be characterized and compared in the temperature range of 4.2 to 70 K. The construction and test of two dimensionally identical non-insulated pancake coils, one dry-wound and one soldered, were presented and compared with a network model. First results showing the behavior of the effective time constant, current distribution and redistributions for current steps, and self-protection were discussed. At 10 K, the average time constant is 1600 higher for the soldered coil than for the dry-wound coil. It was shown that the coil internal voltage behavior can be modelled in regions where the superconducting phase transition is not present, using an equivalent electrical network. The soldered coil operated more stable than the dry wound coil, and as expected self-protection in the case of a quench was observed for the soldered coil in certain conditions.

Acknowledgment

Special thanks to J. Carlos-Perez, J. Mazet, G. Maury, C. Fernandes, N. Bourcey, P.A. Contat, F. Garnier and D. Standen for their aid in design, winding and assembly of the coils. T. Köttig and the cryolab team are thanked for their assistance with the tests. D. Akhmedyanov and R. Mercadillo are thanked for their aid with the design of the magnetic measurement probe.

References

[1] S. Hahn, D. K. Park, J. Bascuñan, and Y. Iwasa, "HTS pancake coils without turn-to-turn insulation," *IEEE Trans. Appl. Supercond.*, vol. 21, no. 3, pp. 1592–1595, Jun. 2011.

[2] Y. Wang, W. K. Chan, and J. Schwartz, "Self-protection mechanism in no-insulation (RE)$Ba_2Cu_3O_x$ high temperature superconductor pancake coils," *Supercon. Sci. Technol.*, vol. 29, no. 4, Mar. 2016, Art. no. 045007.

[3] S. Hahn *et al.*, "Construction and test of 7-T/68-mm cold-bore multiwidth no-insulation GdBCO magnet," *IEEE Trans. Appl. Supercond.*, vol. 25, no. 3, Jun. 2015, Art. no. 4600405.

[4] Y. Li *et al.*, "Feasibility study of the impregnation of a no-insulation HTS coil using solder," *IEEE Trans. Appl. Supercond.*, vol. 28, no. 1, Jan. 2018, Art. no. 5200505.

[5] Y. Q. Li *et al.*, "Study on reducing the charge delay of the no-insulation HTS coil after solder impregnation," *Supercond. Sci. Technol.*, vol. 31, no. 1, Dec. 2017, Art. no. 015018.

[6] J. Ma, J. Geng, and T. A. Coombs, "Flux pumping for non-insulated and metal-insulated HTS coils," *Supercond. Sci. Technol.*, vol. 31, no. 1, Dec. 2017, Art. no. 015018.
[7] S. B. Kim *et al.*, "The characteristics of the normal-zone propagation of the HTS coils with inserted cu tape instead of electrical insulation," *IEEE Trans. Appl. Supercond.*, vol. 22, no. 3, Jun. 2012, Art. no. 4701504.
[8] S. B. Kim *et al.*, "The transient stability of HTS coils with and without the insulation and with the insulation being replaced by Brass tape," *IEEE Trans. Appl. Supercond.*, vol. 23, no. 3, Jun. 2013, Art. no. 7100204.
[9] P. Fazilleau *et al.*, "Metal-as-insulation sub-scale prototype tests under a high background magnetic field," *Supercond. Sci. Technol.*, vol. 31, no. 9, Jul. 2018, Art. no. 095003.
[10] T. Lécrevisse and Y. Iwasa, "A (RE)BCO pancake winding with metal-as-insulation," *IEEE Trans. Appl. Supercond.*, vol. 26, no. 3, Jun. 2016, Art. no. 4700405.
[11] K. Kim *et al.*, "Quench behavior of a no-insulation coil wound with stainless steel cladding REBCO tape at 4.2 K," *Supercond. Sci. Technol.*, vol. 30, no. 7, May 2017, Art. no. 075001.
[12] J. Kim *et al.*, "Effect of resistive metal cladding of HTS tape on the characteristic of no-insulation coil," *IEEE Trans. Appl. Supercond.*, vol. 26, no. 4, Jun. 2016, Art. no. 4601906.
[13] J. Y. Jang *et al.*, "Design, construction and 13 k conduction-cooled operation of a 3 T 100 mm stainless steel cladding all-REBCO magnet," *Supercond. Sci. Technol.*, vol. 30, no. 10, Sep. 2017, Art. no. 105012.
[14] Y. H. Choi *et al.*, "Thermal quench behaviors of no-insulation coils wound using GdBCO coated conductor tapes with various lamination materials," *IEEE Trans. Appl. Supercond.*, vol. 24, no. 3, Jun. 2014, Art. no. 8800105.
[15] Y. J. Hwang, J. Y. Jang, S. Song, J. M. Kim, and S. Lee, "Feasibility study of the impregnation of a no-insulation HTS coil using an electrically conductive epoxy," *IEEE Trans. Appl. Supercond.*, vol. 27, no. 4, Jun. 2017, Art. no. 4603405.
[16] J. van Nugteren, G. Kirby, J. Murtomaki, G. De Rijk, L. Rossi, and A. Stenvall, "Toward REBCO 20 T+ dipoles for accelerators," *IEEE Trans. Appl. Supercond.*, vol. 28, no. 4, Jun. 2018, Art. no. 4008509.
[17] J. Murtomäki, J. van Nugteren, A. Stenvall, G. Kirby, and L. Rossi, "3-D mechanical modeling of 20 t HTS clover leaf end coils—Good practices and lessons learned," *IEEE Trans. Appl. Supercond.*, vol. 29, no. 5, Aug. 2019, Art. no. 4004608.
[18] M. Dam *et al.*, "Conceptual design of a high temperature superconducting magnet for a particle physics experiment in space," *Supercond. Sci. Technol.*, vol. 33, no. 4, Feb. 2020, Art. no. 044012.
[19] E. Felcini *et al.*, "Design of the first HTS single-coil demonstrator of gatoroid toroidal gantry for Hadron therapy," *IEEE Trans. Appl. Supercond.*, vol. 31, no. 5, Aug. 2021, Art. no. 4400205.
[20] S. Richter *et al.*, "High-temperature superconducting undulators for compact free electron lasers," *Verhandlungen der Deutschen Physikalischen Gesellschaft*, vol. 50, no 14, Mar. 2019, Art. no. 50018685.
[21] K. R. Bhattarai, K. Kim, S. Kim, S. Lee, and S. Hahn, "Quench analysis of a multiwidth no-insulation 7-T 78-mm REBCO magnet," *IEEE Trans. Appl. Supercond.*, vol. 27, no. 4, Jun. 2017, Art. no. 4603505.
[22] Y. Yanagisawa *et al.*, "Basic mechanism of self-healing from thermal runaway for uninsulated REBCO pancake coils," *Physica C*, vol. 499, pp. 40–44, Apr. 2014.
[23] T. Wang *et al.*, "Analyses of transient behaviors of no-insulation REBCO pancake coils during sudden discharging and overcurrent," *IEEE Trans. Appl. Supercond.*, vol. 25, no. 3, Jun. 2015, Art. no. 4603409.
[24] H. Song and Y. Wang, "Simulations of non-uniform behaviors of multiple no-insulation (RE)$Ba_2Cu_3O_{7-x}$ pancake coils during charging and discharging," *IEEE Trans. Appl. Supercond.*, vol. 26, no. 4, Jun. 2016, Art. no. 4700105.
[25] W. D. Markiewicz *et al.*, "Quench analysis of pancake wound REBCO coils with low resistance between turns," *Supercond. Sci. Technol.*, vol. 29, no. 2, Dec. 2015, Art. no. 025001.
[26] E. B. Rosa and F. W. Grover, "Formulas and tables for the calculation of mutual and self-inductance," *Bull. Bur. Standards*, vol. 8, no. 1, 1912.
[27] Z. Zhang *et al.*, "An experimental investigation of the transient response of HTS Non-insulation coil," *J. Supercond. Nov. Magn.*, vol. 30, pp. 387–393, Oct. 2016.
[28] Shanghai Superconducting Technology Co., [Online]. Available: http://www.shsctec.com/
[29] Temati, [Online]. Available: https://www.temati-uk.com/site/ccs-performance.html
[30] "High-temperature superconducting wire critical current database," [Online]. Available: http://htsdb.wimbush.eu/
[31] S. Kim, S. Hahn, K. Kim, and D. Larbalestier, "Method for generating linear current-field characteristics and eliminating charging delay in no-insulation superconducting magnets," *Supercond. Sci. Technol.*, vol. 30, no. 3, Feb. 2017, Art. no. 035020.
[32] J. van Nugteren, FIELDS software package.